Hindawi
Journal of Nanomaterials
Volume 2019, Article ID 5429264, 9 pages
https://doi.org/10.1155/2019/5429264

Research Article

Preparation of a Composite Material AC/Cu-BTC with Improved Water Stability and n-Hexane Vapor Adsorption

Manlin Li,[1] Weiqiu Huang,[1] Bo Tang,[1] Fujiao Song,[2] Aihua Lv,[1,3] and Xiang Ling[3]

[1]*Jiangsu Key Laboratory of Oil & Gas Storage and Transportation Technology, Changzhou University, Changzhou 213164, China*
[2]*School of Environmental Science and Engineering, Yancheng Institute of Technology, Yancheng 224051, China*
[3]*Jiangsu Key Laboratory of Process Enhancement and New Energy Equipment Technology, Nanjing Tech University, Nanjing 211816, China*

Correspondence should be addressed to Weiqiu Huang; hwq213@cczu.edu.cn and Xiang Ling; xling@njtech.edu.cn

Received 1 May 2019; Accepted 5 August 2019; Published 10 September 2019

Academic Editor: Nageh K. Allam

The Cu-BTC, a widely studied metal-organic framework (MOF), has been applied in various fields such as gas adsorption, separation, storage, and catalysis. However, the Cu-BTC collapses due to the replacement of the organic linker by water molecules under humid conditions, which limits its practical application in industries. In consideration of the undesirable water effect on the framework stability of Cu-BTC, a stable activated carbon (AC) was incorporated into it by the in situ method to yield a composite material AC/Cu-BTC with high water stability. XRD and SEM patterns proved that the $AC_{7\%}$/Cu-BTC successfully retains its crystal structure after being exposed to water molecules. The adsorption amount of n-hexane vapor of the $AC_{7\%}$/Cu-BTC after water vapor adsorption-thermal desorption is 307% of that of the Cu-BTC. The addition of the AC changes the adsorption active sites and reduces the strong affinity of the Cu-BTC to water molecules, resulting in the $AC_{7\%}$/Cu-BTC having a much lower adsorption rate for water vapor than the Cu-BTC. Therefore, the $AC_{7\%}$/Cu-BTC can be protected from a large amount of water molecules and avoid structural collapse caused by the disconnection between the copper center and the organic linker. The composite displays a potential value for stable applications of MOF-based materials under ambient conditions.

1. Introduction

The continuously increasing amount of volatile organic compounds (VOCs) due to the exploitation, storage, refining, transport, and usage of fossil fuels has severely threatened human health and the ecological environment [1–3]. VOCs include alkanes, aromatics, and organic alcohols. Usually, n-hexane is regarded as a representative of alkanes [4]. While the search for alternative clean energy sources continues, developing new adsorbents for VOC adsorption and sequestration is still necessary and has significant impact on controlling VOCs. Metal-organic frameworks (MOFs) have been recognized as promising porous materials for high specific surface area, large pore volume, and good thermal stability [5–7], and have been applied in various fields such as gas storage, separation/adsorption, and catalysis [8–12]. The multiple options for the metal centers and linkers enable the rational design and synthesis of MOF structures to achieve enhanced adsorption capacities [13]. Within the class of MOFs, copper-benzene-1,3,5-tricarboxylate (Cu-BTC), also known as HKUST-1 [14], is a well-studied structure, which has shown promising performance for VOC adsorption. With minimized water exposure, the Cu-BTC has high adsorption capacities [15–17], exceeding $0.65\,cm^3 \cdot g^{-1}$ for methanol, acetone, acetonitrile, n-hexane, and m-xylene.

Water vapor is inevitable in industrial applications, especially during the VOC recovery process, which must be taken into account [18] when selecting the adsorbent for the adsorption separation and purification system. MOF behavior in the presence of water plays a significant role when considering these materials for adsorption applications. Although the Cu-BTC has certain water stability, it is sensitive to humid streams, leading to dynamic deformation of its porous structure. Molecules with high dipole moments, such as water [19], are preferentially adsorbed in cages containing the open metal sites. Under humid condition, water

displaces the organic linkers from the copper centers, causing the collapse of the Cu-BTC.

At present, a number of groups are concentrating on improving the water stability of MOFs. The most widely used solutions are incorporating chemicals to introduce new groups to protect Cu sites. There are several approaches to improve the water stability of MOFs. Lin et al. [20] proposed a postsynthetic strategy to introduce acetonitrile (ACN) into the Cu-BTC to form ACN/Cu-BTC, which completely inhibited the water-induced adsorptive capacity degeneration. In addition to utilizing hydrophobicity as a barrier to exclude water from entering the pore on the external crystal surface, it is a good alternative to introduce hydrophobic groups on the inner surface of the structure. Gutiérrez-Sevillano et al. [21] suggested that the hydrophobic groups can be used to shield the weakest point of the structure to improve the water stability of the framework. Li et al. [22] proposed a strategy that the Cu-BTC was functionalized with imidazole (IMI) for enhancing its steam stability using a new ultrafast room temperature synthesis method. Yu et al. [23] used copper nitrate as the metal ion source and BTC-(n)Br as an organic ligand and successfully synthesized a new type of hydrophobic adsorbent, Cu-BTC-(n)Br, by the hydrothermal method, which shows distinguished hydrophobicity and remarkable adsorption effectivity under aqueous circumstance.

All the above-mentioned approaches for improving the water stability of the Cu-BTC need to introduce chemicals, which are generally toxic or unfriendly to the environment and humans. In view of these shortcomings, this study tried to seek other environment-friendly alternatives. AC is one of the earliest and widest applied conventional adsorbents with stable performance and corrosion resistance. The AC is hydrophobic and it has a nonpolar surface with affinity for organic matter [24]. Traditional and new adsorbents have their own advantages and disadvantages and combing them together may produce unexpected results. Azad et al. [25] prepared AC-HKUST-1 by ultrasonic-assisted hydrothermal method and applied the obtained product for the simultaneous ultrasound-assisted removal of crystal violet (CV), disulfide blue (DSB), and quinoline yellow (QY) dyes in their ternary solution. Esfandiari et al. [26] investigated the effect of incorporating AC as a void space filling agent in the Cu-BTC structure on hydrogen uptake.

In this work, we creatively combined the traditional adsorbent AC with the new adsorbent Cu-BTC utilizing the in situ hydrothermal method, greatly improving the water stability of the Cu-BTC. Activated carbon itself has adsorption properties, which can adsorb Cu^{2+} and change the active sites of the Cu-BTC, reducing its affinity for water. A series of AC/Cu-BTCs with different AC contents were prepared. Scanning electron microscopy (SEM) was used to observe the changes of the macroscopic structure. The moisture stability of AC/Cu-BTC was evaluated by the XRD analysis, measuring the samples before and after being exposed to humidity for 2 months. The n-hexane vapor adsorption capacities of the Cu-BTC and AC/Cu-BTC before and after adsorbing-heat desorbing water vapor were also studied under room temperature and atmospheric pressure. At the same time, the water vapor adsorption and desorption rates were investigated.

2. Materials and Methods

2.1. Materials. Copper (II) nitrate trihydrate ($Cu(NO_3)_2{\cdot}3H_2O$, 99.5%) was purchased from Nicechem, and benzene-1,3,5-tricarboxylic acid (BTC, 95%) was obtained from Aladdin. Ethanol (absolute) and N,N-dimethylformamide (DMF) were provided by Guoyao Chemicals Co. Ltd. Activated carbon (MZ02) was acquired from Fujian Xinsen Carbon Co. Ltd. All materials were used as received without further purification.

2.2. Synthesis of the Cu-BTC and AC/Cu-BTC. The general procedure of preparing the Cu-BTC using hydrothermal synthesis was based on the method reported by Rowsell and Yaghi [27], with a slight change. 2.078 g copper (II) nitrate trihydrate and 15 mL distilled water were mixed and stirred evenly. 1.002 g BTC was dissolved in 30 mL mixture of ethanol and DMF in 1 : 1 vol% with stirring. Then, the two solutions were mixed and stirred for 10 min with a magnetic stirrer. The mixture was then transferred into a 100 mL Teflon-lined stainless steel autoclave and heated in an oven at 373 K for 10 h. After cooling to room temperature normally, the solution was centrifuged and some blue solid product was attained. The solid was washed with ethanol to remove unreacted materials, activated for one day, and then dried at 353 K for 6 h.

To obtain the AC/Cu-BTC, the Cu-BTC parent solution was fully mixed with the AC by the in situ method. A certain amount of the AC powder in some AC/Cu-BTC ratio was mixed with the parent solutions and stirred for 0.5 h until mixed evenly, named $AC_{5\%}$/Cu-BTC, $AC_{7\%}$/Cu-BTC, and $AC_{10\%}$/Cu-BTC. Then, the resulting dark blue mixture was transferred into a 100 mL Teflon-lined stainless steel autoclave and heated at 373 K for 10 h. The reactor was cooled to room temperature after synthesis, crystallizing and producing blue powder. The powder was then filtered, washed, and activated thoroughly with ethanol for one day. The product was finally dried for 6 h in an oven at 353 K.

2.3. Characterizations of the AC/Cu-BTC. X-ray diffraction (XRD) was recorded on a MAX2500 X-ray diffractometer with Cu Ka emission at room temperature with a scan speed of 2° min^{-1} and a step size of 0.02°. Scanning electron microscopy (SEM) analyses were carried out using a ZEISS SUPRA-55 emission scanning electron microscope with a high voltage mode of 15 kV. The FT-IR spectra of compounds were recorded on a Thermo Fisher */IS50 instrument. N_2 isotherms at 77 K were obtained with an automated gas sorption analyzer (Quantachrome). The degassing was carried out at 423 K overnight under vacuum prior to the measurement. Thermogravimetric analyses (TGA) were carried out with a METTLER thermogravimetric analyzer. The temperature range was 303 to 800 K with a heating rate of 10 K·min^{-1} in a nitrogen atmosphere (50 mL·min^{-1}).

2.4. Water and n-Hexane Vapor Adsorption. The adsorption capacities of the AC/Cu-BTCs and Cu-BTC on hexane

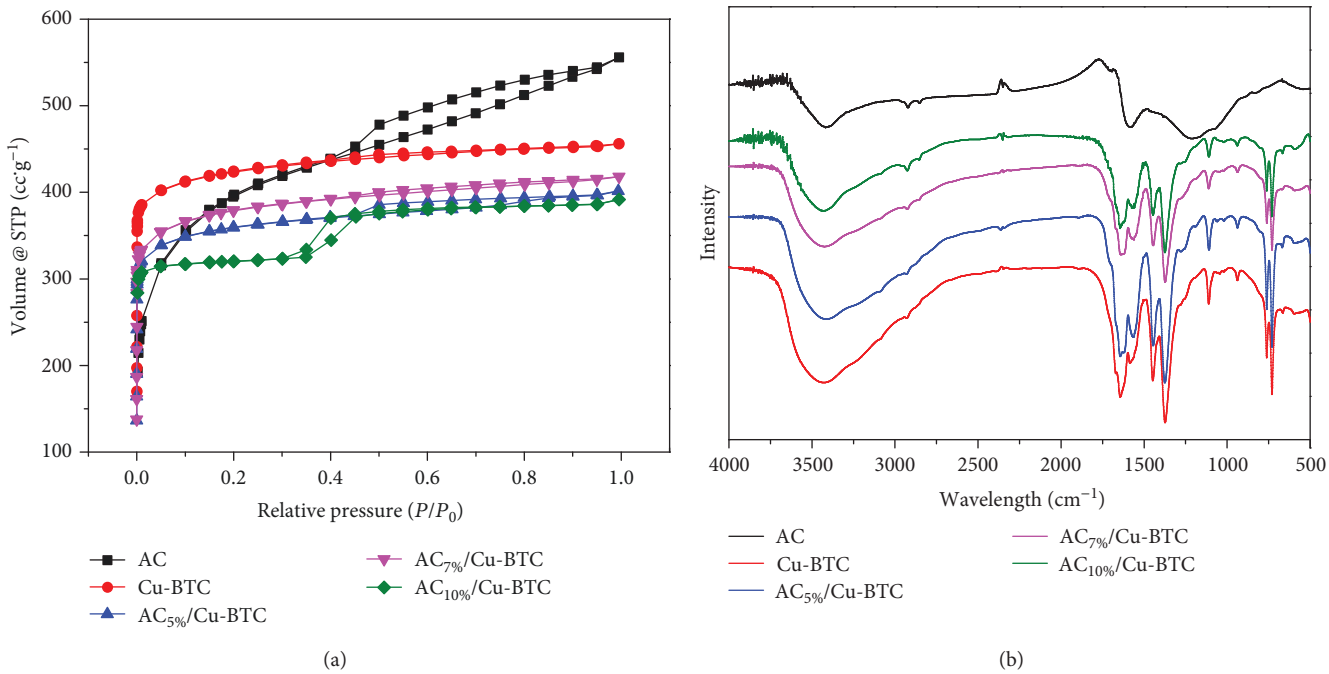

Figure 1: (a) N_2 isotherms at 77 K; (b) FT-IR of the Cu-BTC and AC/Cu-BTCs.

vapor were tested with a thermogravimetric analyzer (TGA/DSC3+, METTLER), which can determine the adsorption capacity and heat of adsorption at the same time. The water and n-hexane were diluted with nitrogen (99.999%) under atmospheric pressure. Samples which have been produced for a period of time were taken 8 to 10 mg and placed in 150 μL ceramic crucibles. All samples were treated at 423 K for 1 h before measurement. In order to be consistent with industrial adsorption conditions, the adsorption temperature was set as 303 K and the pressure was atmospheric. A thermogravimetric analyzer can keep the adsorption temperature constant. The sample firstly adsorbed water at 50 mL·min^{-1}. After the water adsorption, it was thermally desorbed at 423 K, and then the n-hexane was adsorbed under the same conditions.

3. Results and Discussion

3.1. Characterizations of the AC/Cu-BTC. Figure 1(a) compares the N_2 isotherms of the Cu-BTC and AC/Cu-BTCs at 77 K. The N_2 isotherms of the selected AC contain a hysteresis loop, meaning the presence of mesopores. The synthesis process is carried out at a certain temperature, pressure, and acidity. Under these conditions, a sufficient amount of the AC has a nonnegligible effect on the crystallization of the Cu-BTC, such as plugging its pores and introducing mesopores. The surface area parameters of the samples are listed in Table 1, which were calculated with the built-in software of Quantachrome. The results in Table 1 indicate that the specific surface areas of the AC/Cu-BTCs are lower than that of the pristine MOF. This can be attributed to the introduction of the AC.

FT-IR was conducted to analyze the functional groups present in the Cu-BTC and their status after the incorporation of the AC into the Cu-BTC. FT-IR patterns of the AC, Cu-BTC, and AC/Cu-BTC are shown in Figure 1(b). FT-IR indicates that there is no new functional group formation between the AC and the Cu-BTC. FT-IR spectra of the Cu-BTC show a broad bond at 3423 cm^{-1} and 1374 cm^{-1} corresponding to hydrogen-bonded –OH stretching and bending vibrations, thanks to the adsorbed water on the surface of the samples. The AC is less hydrophilic than the Cu-BTC. Water molecules have large dipole moments and therefore have a strong affinity for the copper center. Under humid condition, water molecules displace the organic linkers from the copper centers, causing the collapse of the Cu-BTC framework [5].

Table 1: Surface area parameters of the Cu-BTC and AC/Cu-BTCs.

Sample	BET surface area ($m^2 \cdot g^{-1}$)	Langmuir surface area ($m^2 \cdot g^{-1}$)	AC content
Cu-BTC	1663	1902	/
AC	1420	1960	/
AC$_{5\%}$/Cu-BTC	1404	1620	16.73%
AC$_{7\%}$/Cu-BTC	1469	1715	23.90%
AC$_{10\%}$/Cu-BTC	1339	1413	22.97%

The XRD patterns of the fresh Cu-BTC and AC/Cu-BTCs are shown in Figure 2(a). All three composites have similar characteristic peaks as the Cu-BTC, suggesting that the AC/Cu-BTCs maintain the microstructure of the Cu-BTC. The variations in intensities of the different diffraction peaks can be attributed to the degree of hydration of different samples, which is due to the Cu-BTC being able to rapidly adsorb moisture from the air. In addition, the

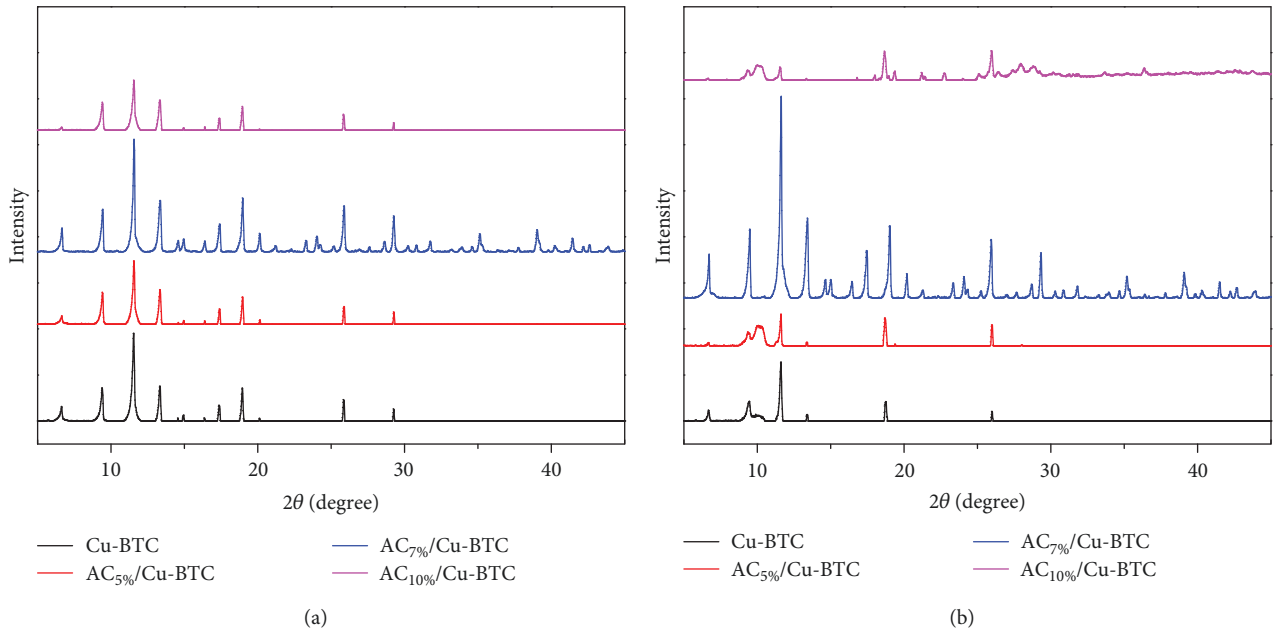

Figure 2: (a) XRD patterns of the fresh AC/Cu-BTC; (b) XRD patterns of the AC/Cu-BTCs exposed to moisture for two months.

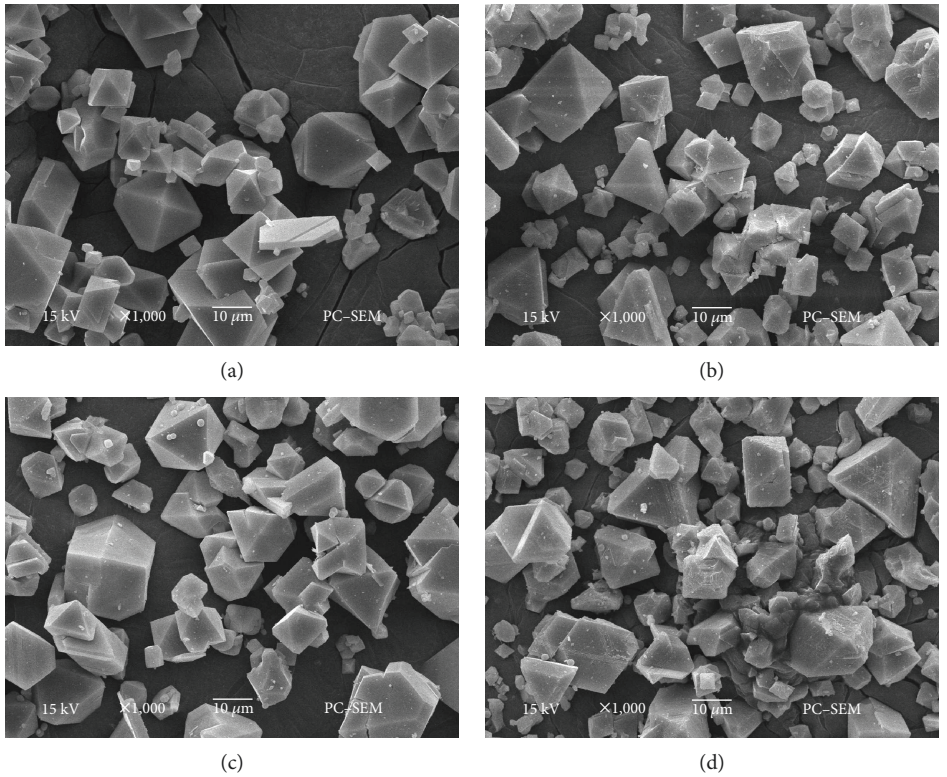

Figure 3: SEM images of the samples: (a) Cu-BTC, (b) $AC_{5\%}$/Cu-BTC, (c) $AC_{7\%}$/Cu-BTC, and (d) $AC_{10\%}$/Cu-BTC.

presence of the AC also has a negligible effect on the water adsorption rate of the Cu-BTC, which contributes to the difference of the diffraction peaks.

The SEM images in Figure 3 reveal the morphologies of the AC/Cu-BTCs. It can be seen that the $AC_{5\%}$/Cu-BTC and $AC_{7\%}$/Cu-BTC have little change in morphology compared with the Cu-BTC, while the $AC_{10\%}$/Cu-BTC crystals are stacked and adhered. When the added AC content is over a certain amount, it would lead to much larger crystal size and close packing of the Cu-BTC crystal. The AC is an

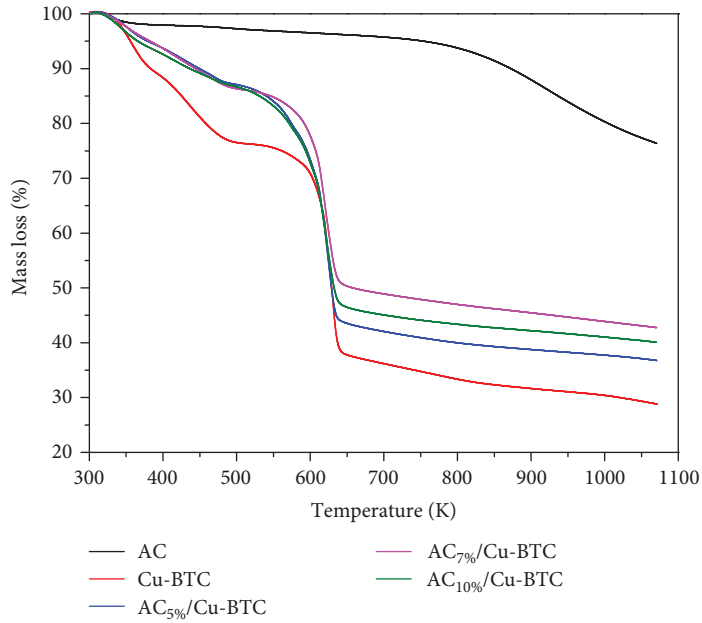

Figure 4: TGA of the AC/Cu-BTCs.

amorphous carbon with no much functional groups on the surface, which can provide a place for strong binding interactions for nucleation, growth, and adhesion of MOF crystals.

The actual AC percentages in the composites are calculated via TGA results, and the equations are as follows:

$$1 = \omega_{\text{Cu-BTC\%}} + \omega_{\text{AC\%}}, \quad (1)$$

$$\omega_{\text{Residue\%}} = 0.2881\omega_{\text{Cu-BTC\%}} + 0.7683\omega_{\text{AC\%}}, \quad (2)$$

where $\omega_{\text{Cu-BTC\%}}$ and $\omega_{\text{AC\%}}$ are the actual weight percentages of the Cu-BTC and the AC in the composites, respectively. $\omega_{\text{Residue\%}}$ is the actual weight percentage of the residue in composites, and 0.2881 and 0.7683 are the weight fractions of the residue of the pure Cu-BTC and AC, respectively. The results are presented in Figure 4 and Table 1. The calculation results indicate that $AC_{5\%}$/Cu-BTC contains the least amount of AC and $AC_{7\%}$/Cu-BTC contains the most. The possible reason is that the AC impacts the crystallization process of the Cu-BTC and thus affects the productivity. Excessive AC hinders the formation of the Cu-BTC crystals, causing some of the reactants to not react and be washed away during the cleaning process. Therefore, the actual AC content of $AC_{10\%}$/Cu-BTC is lower than that of $AC_{7\%}$/Cu-BTC.

3.2. Improved Water Stability of the AC/Cu-BTC. Lin et al. and Li et al. [20, 22] reported that the Cu-BTC lost most of its crystallinity after several days' exposure in moisture. Considering these and some conditions of the VOC recovery, the AC/Cu-BTCs have been exposed to humidity for 2 months under ambient conditions. The XRD patterns of the samples after being exposed to humidity for 2 months are exhibited in Figure 2(b). The characteristic peaks of AC/Cu-BTCs at $2\theta \approx 6.5^\circ$, 9.5°, 11.5°, and 13.4° are recognizable, suggesting the AC/Cu-BTCs maintain the microstructure. Contrary to the experimental results of Lin et al. and Li et al., the Cu-BTC synthesized in this work still retains its characteristic peaks, which probably can be attributed to the difference in solvent concentration, reaction temperature, and time. Merely investigating the effect of humidity on the XRD of the AC/Cu-BTCs is not sufficient to demonstrate the effect of the AC on the water stability of the Cu-BTC.

The n-hexane vapor adsorption curves of the fresh and used Cu-BTC and AC/Cu-BTCs are compared to further evaluate their water stability. Figure 5 and Table 2 present n-hexane vapor adsorption curves before and after adsorbing water. The n-hexane vapor adsorption capacity of the Cu-BTC is 3.52 $\text{mmol}\cdot\text{g}^{-1}$, which only retains 0.65 $\text{mmol}\cdot\text{g}^{-1}$ after adsorbing water vapor, while the $AC_{7\%}$/Cu-BTC preserves 81% of its initial n-hexane vapor adsorption capacity, from 2.47 $\text{mmol}\cdot\text{g}^{-1}$ to 2.00 $\text{mmol}\cdot\text{g}^{-1}$, which is 307% of that of the Cu-BTC. The AC has excellent water stability, and the adsorption capacity to n-hexane vapor is almost unchanged after undergoing water vapor adsorption. Simultaneously, both $AC_{5\%}$/Cu-BTC and $AC_{10\%}$/Cu-BTC after water vapor adsorption have much higher adsorption capacities than the Cu-BTC.

The AC provides a place for strong binding interactions for nucleation, growth, and adhesion of the Cu-BTC crystals, which has an influence on its surface area parameters. As a result, the specific surface area of Cu-BTC is reduced and the original n-hexane adsorption capacity is reduced. The selected AC is hydrophobic and water stable, which was well inherited by the AC/Cu-BTC, especially the $AC_{7\%}$/Cu-BTC, retaining most of the adsorption capacity of the Cu-BTC for n-hexane vapor.

From the FT-IR results, no new functional groups were generated between the AC and the Cu-BTC, excluding the

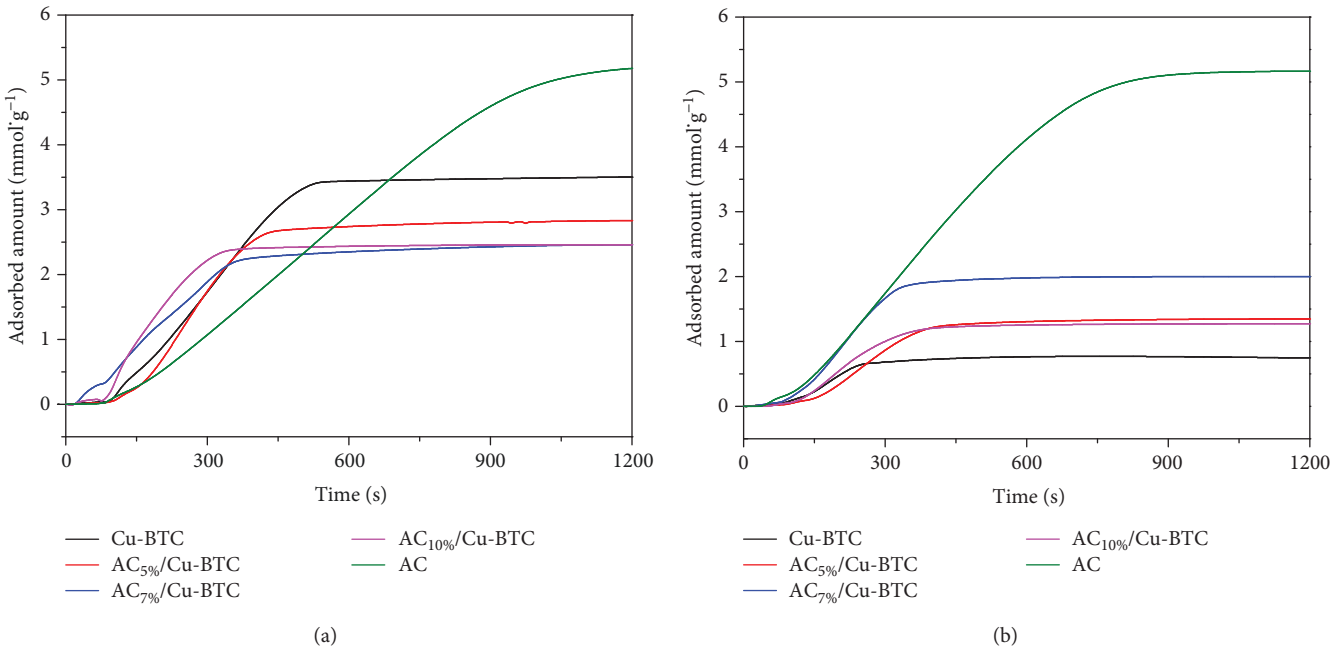

Figure 5: (a) n-Hexane vapor adsorption of the fresh AC/Cu-BTCs and (b) n-hexane vapor adsorption of the AC/Cu-BTCs after adsorbing-heat desorbing water vapor.

Table 2: n-Hexane vapor adsorption of the Cu-BTC and AC/Cu-BTCs.

Sample	Fresh (mmol·g^{-1})	Used* (mmol·g^{-1})
Cu-BTC	3.52	0.65
AC	5.25	5.17
AC$_{5\%}$/Cu-BTC	2.83	1.35
AC$_{7\%}$/Cu-BTC	2.47	2.00
AC$_{10\%}$/Cu-BTC	2.45	1.27

*The used adsorbents herein mean that the adsorbents had firstly adsorbed the water vapor and then were desorbed by heat under the N_2 atmosphere.

influence of hydrophobic functional groups. However, the water stability of the AC/Cu-BTC is indeed improved, which is manifested by the fact that the amount of n-hexane after water adsorption is much higher than that of the Cu-BTC. Therefore, the AC definitely has effects on Cu-BTC. According to the adsorption results, we speculated that the presence of the AC alters the adsorption active sites of the Cu-BTC for water and weakens its hydrophilicity. If so, the water adsorption rate and desorption temperature of the AC$_{7\%}$/Cu-BTC must be lower than those of the Cu-BTC.

The water vapor adsorption and desorption rates of the AC$_{7\%}$/Cu-BTC are shown in Figure 6. It can be seen from Figure 6(a) that the maximum water adsorption capacity of the Cu-BTC is 22 mmol·g^{-1} and 1.9 mmol·g^{-1}·min^{-1}, while that of the AC$_{7\%}$/Cu-BTC is 14 mmol·g^{-1} and 1.1 mmol·g^{-1}·min^{-1}, meaning that the Cu-BTC has a significantly stronger affinity to water than the AC$_{7\%}$/Cu-BTC. In addition, Figure 6(b) indicates that the water desorption rate of the AC$_{7\%}$/Cu-BTC is greater than that of the Cu-BTC. Under the same temperature condition, the AC$_{7\%}$/Cu-BTC can quickly remove large amounts of water molecules. Therefore, it can be concluded that the addition of the AC reduces the hydrophilicity of the Cu-BTC.

The SEM images in Figure 7 display the structure of the Cu-BTC and AC$_{7\%}$/Cu-BTC after water adsorption. It can be seen from Figure 7 that the Cu-BTC framework collapses after water vapor adsorption. Figure 8 explains the mechanism of how the AC protects the crystal structure. The Cu-BTC is sensitive to humid streams in that water can displace the organic linkers from the copper centers and its porous structure dynamically collapses at certain temperature and various relative humidity values, contributing to the irreversible decomposition of the Cu-BTC framework. As a consequence, the adsorption capacity inevitably deteriorates [5, 21]. However, the AC$_{7\%}$/Cu-BTC still maintains its crystal structure; only the surface is eroded by water. The AC does improve the water stability of the Cu-BTC. The possible reason is that the adsorption active sites of the AC$_{7\%}$/Cu-BTC are different from those of the Cu-BTC, which may be distributed on the surface. Thus, the affinity and bonding to water molecules of the AC$_{7\%}$/Cu-BTC is decreased, protecting the structure from being destroyed by water molecules.

Figure 8 describes the mechanism of how the AC protects the crystal structure of the Cu-BTC. The Cu-BTC is hydrophilic in that it can quickly adsorb a large amount of water molecules, which can replace the organic linker, leading to the collapse of the Cu-BTC. The participation of the AC relieves the damage of water to the Cu-BTC. The AC$_{7\%}$/Cu-BTC inherits the hydrophobic properties of the AC and weakens the affinity of the Cu-BTC to water molecules. In addition, a large amount of water molecules can rapidly penetrate the Cu-BTC crystal. The presence of the AC slows down

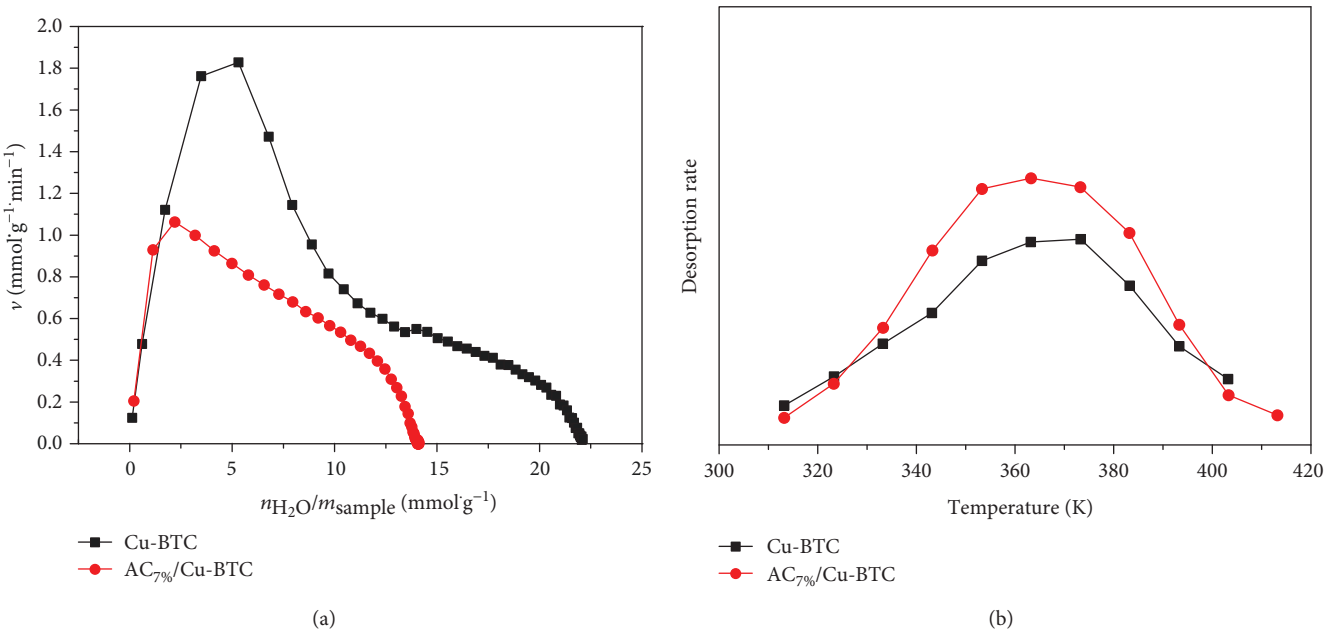

Figure 6: (a) Water vapor adsorption rate of the Cu-BTC and $AC_{7\%}$/Cu-BTC and (b) water desorption of the Cu-BTC and $AC_{7\%}$/Cu-BTC.

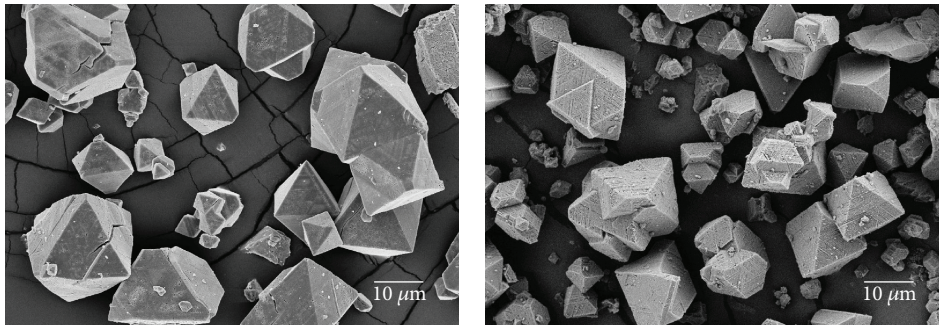

Figure 7: SEM images of the samples after adsorbing-heat desorbing water: (a) Cu-BTC; (b) $AC_{7\%}$/Cu-BTC.

this process and reduces the adsorption rate of the Cu-BTC on water molecules, so that water molecules can only erode its surface instead of penetrating the Cu-BTC crystal. Therefore, the $AC_{7\%}$/Cu-BTC can preserve its crystal structure.

4. Conclusions

In summary, a new strategy was proposed to improve the water stability of the Cu-BTC by incorporating the AC into it with the in situ method. The AC successfully improved the water stability of the Cu-BTC. The $AC_{7\%}$/Cu-BTC retained its crystal structure intact after exposure to humid air for two months. The adsorption capacity of the $AC_{7\%}$/Cu-BTC for n-hexane under ambient conditions is slightly lower than that of the Cu-BTC. Interestingly, the adsorption capacity of $AC_{7\%}$/Cu-BTC for n-hexane is three times that of the Cu-BTC after water adsorption. Furthermore, the presence of AC reduces the adsorption rate of the Cu-BTC to water and weakens the damage of the Cu-BTC macrostructure by water molecules. The enhanced water resistance stability is promising for MOF adsorbents in moisture applications.

Data Availability

The authors give permission for the publisher and readers to access all data related to the findings in this article. Any accessibility to all data is open for readers, and these included the following: Figure 1: (a) N2 isotherms at 77 K and (b) FT-IR of the Cu-BTC and AC/Cu-BTC; Figure 2: (a) XRD patterns of the fresh AC/Cu-BTC and (b) XRD patterns of the AC/Cu-BTCs exposed to moisture two months; Figure 3: SEM images of the samples ((a) Cu-BTC, (b) $AC_{5\%}$/Cu-BTC, (c) $AC_{7\%}$/Cu-BTC, and (d) $AC_{10\%}$/Cu-BTC); Figure 4: TGA of the AC/Cu-BTCs; Figure 5: (a) N-hexane adsorption of the fresh AC/Cu-BTCs and (b) N-hexane adsorption of the AC/Cu-BTCs after adsorbing-heat desorbing water; Figure 6: (a) water adsorption rate of the AC/Cu-BTCs and (b) water desorption of the Cu-BTC

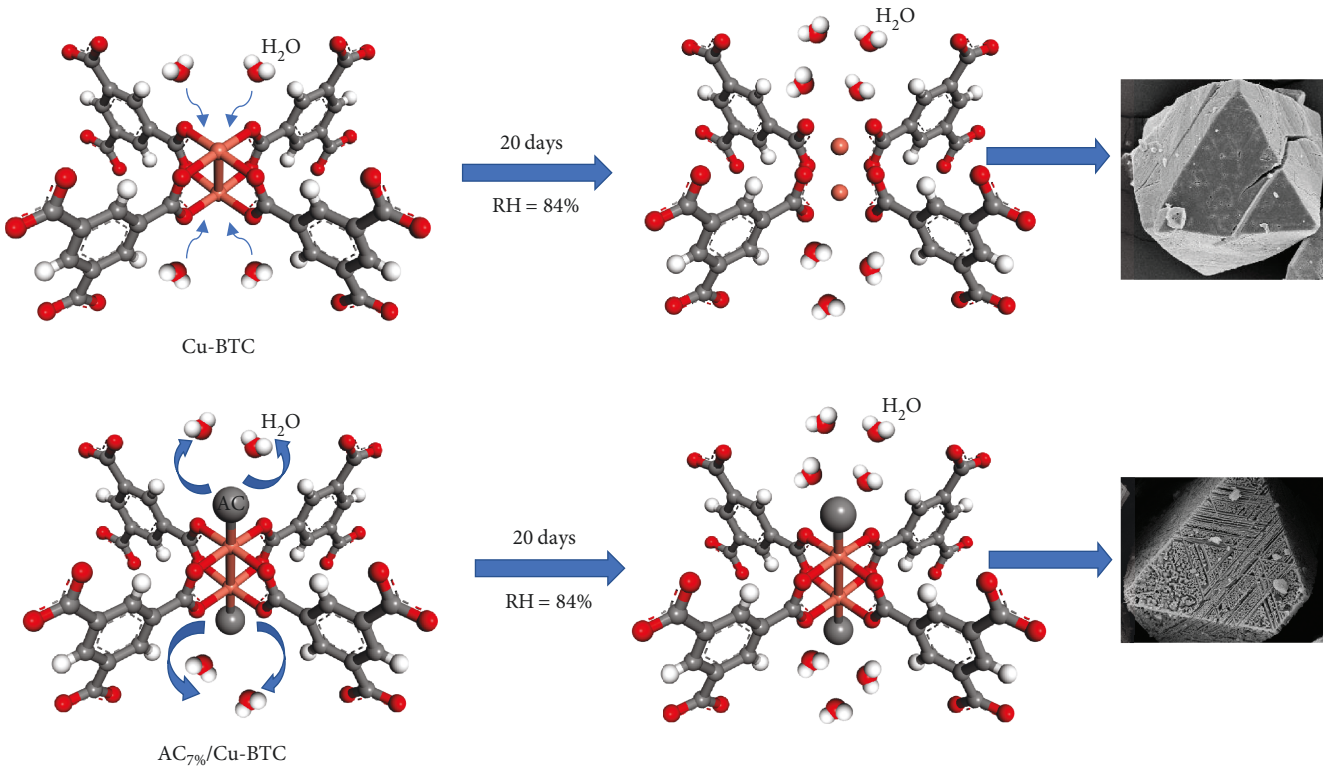

Figure 8: The mechanism of how the AC protects the crystal structure.

and $AC_{7\%}$/Cu-BTC; and Figure 7: SEM images of the samples after adsorbing-heat desorbing water ((a) Cu-BTC; (b) $AC_{7\%}$/Cu-BTC) which were presented in the finding of this study are raw data, and they were not published elsewhere and may be released upon application to the Jiangsu Key Laboratory of Oil & Gas Storage and Transportation Technology, Changzhou University, Changzhou 213164, China, where they can contact Professor Weiqiu Huang (hwq213@cczu.edu.cn). (2) All the data used to support the findings of this study are available and have been included within the article.

Conflicts of Interest

The authors declare that they have no conflicts of interest.

Acknowledgments

This work was supported by the National Natural Science Foundation of China (Nos. 51574044 and 51576095). This work was also supported by the Key Research and Development Program of Jiangsu Province (Industry Foresight and Common Key Technology, No. BE2018065).

References

[1] P. Harb, N. Locoge, and F. Thevenet, "Emissions and treatment of VOCs emitted from wood-based construction materials: impact on indoor air quality," *Chemical Engineering Journal*, vol. 354, no. 85, pp. 641–652, 2018.

[2] A. H. Jalal, F. Alam, S. Roychoudhury, Y. Umasankar, N. Pala, and S. Bhansali, "Prospects and challenges of volatile organic compound sensors in human healthcare," *ACS Sensors*, vol. 3, no. 7, pp. 1246–1263, 2018.

[3] X. Zhang, B. Gao, A. E. Creamer, C. Cao, and Y. Li, "Adsorption of VOCs onto engineered carbon materials: a review," *Journal of Hazardous Materials*, vol. 338, no. 13, pp. 102–123, 2017.

[4] M. S. Kamal, S. A. Razzak, and M. M. Hossain, "Catalytic oxidation of volatile organic compounds (VOCs)-a review," *Atmospheric Environment*, vol. 140, no. 31, pp. 117–134, 2016.

[5] N. Al-Janabi, P. Hill, L. Torrente-Murciano et al., "Mapping the Cu-BTC metal–organic framework (HKUST-1) stability envelope in the presence of water vapour for CO_2 adsorption from flue gases," *Chemical Engineering Journal*, vol. 281, pp. 669–677, 2015.

[6] L. Feng, R. Chen, S. Hou et al., "Common but differentiated flexible MIL-53(Al): role of metal sources in synthetic protocol for tuning the adsorption characteristics," *Journal of Materials Science*, vol. 54, no. 8, pp. 6174–6185, 2019.

[7] Y. Liu, P. Ghimire, and M. Jaroniec, "Copper benzene-1,3,5-tricarboxylate (Cu-BTC) metal-organic framework (MOF) and porous carbon composites as efficient carbon dioxide adsorbents," *Journal of Colloid and Interface Science*, vol. 535, pp. 122–132, 2019.

[8] K. Peikert, F. Hoffmann, and M. Froba, "Amino substituted $Cu_3(btc)_2$: a new metal–organic framework with a versatile functionality," *Chemical Communications*, vol. 48, no. 91, pp. 11196–11198, 2012.

[9] T. Terencio, F. di Renzo, D. Berthomieu, and P. Trens, "Adsorption of acetone vapor by Cu-BTC: an experimental

and computational study," *Journal of Physical Chemistry C*, vol. 117, no. 49, pp. 26156–26165, 2013.

[10] T. Dutta, K. H. Kim, R. J. C. Brown, Y. H. Kim, and D. Boukhvalov, "Metal-organic framework and Tenax-TA as optimal sorbent mixture for concurrent GC-MS analysis of C1 to C5 carbonyl compounds," *Scientific Reports*, vol. 8, no. 1, p. 5033, 2018.

[11] A. W. Stubbs, L. Braglia, E. Borfecchia et al., "Selective catalytic olefin epoxidation with Mn^{II}-exchanged MOF-5," *ACS Catalysis*, vol. 8, no. 1, pp. 596–601, 2018.

[12] N. A. A. Qasem, R. Ben-Mansour, and M. A. Habib, "An efficient CO_2 adsorptive storage using MOF-5 and MOF-177," *Applied Energy*, vol. 210, no. 11, pp. 317–326, 2018.

[13] T. M. Tovar, J. Zhao, W. T. Nunn et al., "Diffusion of CO_2 in large crystals of Cu-BTC MOF," *Journal of the American Chemical Society*, vol. 138, no. 36, pp. 11449–11452, 2016.

[14] S. S. Y. Chui, S. M. F. Lo, J. P. Charmant, A. G. Orpen, and I. D. Williams, "A chemically functionalizable nanoporous material $[Cu_3(TMA)_2(H_2O)_3]_n$," *Science*, vol. 283, no. 5405, pp. 1148–1150, 1999.

[15] T. R. C. Van Assche, T. Duerinck, J. J. Gutiérrez Sevillano, S. Calero, G. V. Baron, and J. F. M. Denayer, "High adsorption capacities and two-step adsorption of polar adsorbents on copper–benzene-1,3,5-tricarboxylate metal–organic framework," *The Journal of Physical Chemistry C*, vol. 117, no. 35, pp. 18100–18111, 2013.

[16] Z. Hulvey, B. Vlaisavljevich, J. A. Mason et al., "Critical factors driving the high volumetric uptake of methane in $Cu_3(btc)_2$," *Journal of the American Chemical Society*, vol. 137, no. 33, pp. 10816–10825, 2015.

[17] N. Klein, A. Henschel, and S. Kaskel, "n-Butane adsorption on $Cu_3(btc)_2$ and MIL-101," *Microporous and Mesoporous Materials*, vol. 129, no. 1-2, pp. 238–242, 2010.

[18] N. C. Burtch, H. Jasuja, and K. S. Walton, "Water stability and adsorption in metal–organic frameworks," *Chemical Reviews*, vol. 114, no. 20, pp. 10575–10612, 2014.

[19] J. M. Castillo, T. J. H. Vlugt, and S. Calero, "Understanding water adsorption in Cu-BTC metal-organic frameworks," *Journal of Physical Chemistry C*, vol. 112, no. 41, pp. 15934–15939, 2008.

[20] Z. Lin, Z. Lv, X. Zhou, H. Xiao, J. Wu, and Z. Li, "Postsynthetic strategy to prepare ACN@Cu-BTCs with enhanced water vapor stability and CO_2/CH_4 separation selectivity," *Industrial & Engineering Chemistry Research*, vol. 57, no. 10, pp. 3765–3772, 2018.

[21] J. J. Gutiérrez-Sevillano, D. Dubbeldam, L. Bellarosa et al., "Strategies to simultaneously enhance the hydrostability and the alcohol–water separation behavior of Cu-BTC," *The Journal of Physical Chemistry C*, vol. 117, no. 40, pp. 20706–20714, 2013.

[22] H. Li, Z. Lin, X. Zhou et al., "Ultrafast room temperature synthesis of novel composites Imi@Cu-BTC with improved stability against moisture," *Chemical Engineering Journal*, vol. 307, no. 128, pp. 537–543, 2017.

[23] L. Yu, Q. Liu, W. Dai, N. Tian, and N. Ma, "Efficient thiophene capture with a hydrophobic Cu-BTC-(n)Br adsorbent in the presence of moisture," *Microporous and Mesoporous Materials*, vol. 266, no. 32, pp. 7–13, 2018.

[24] G. Le Bozec, S. Giraudet, L. Le Polles, and P. Le Cloirec, "^{1}H NMR investigations of activated carbon loaded with volatile organic compounds: quantification, mechanisms, and diffusivity determination," *Langmuir*, vol. 33, no. 7, pp. 1605–1613, 2017.

[25] F. N. Azad, M. Ghaedi, K. Dashtian, S. Hajati, and V. Pezeshkpour, "Ultrasonically assisted hydrothermal synthesis of activated carbon–HKUST-1-MOF hybrid for efficient simultaneous ultrasound-assisted removal of ternary organic dyes and antibacterial investigation: Taguchi optimization," *Ultrasonics Sonochemistry*, vol. 31, no. 24, pp. 383–393, 2016.

[26] K. Esfandiari, A. R. Mahdavi, A. A. Ghoreyshi, and M. Jahanshahi, "Optimizing parameters affecting synthetize of CuBTC using response surface methodology and development of AC@CuBTC composite for enhanced hydrogen uptake," *International Journal of Hydrogen Energy*, vol. 43, no. 13, pp. 6654–6665, 2018.

[27] J. L. C. Rowsell and O. M. Yaghi, "Effects of functionalization, catenation, and variation of the metal oxide and organic linking units on the low-pressure hydrogen adsorption properties of metal-organic frameworks," *Journal of the American Chemical Society*, vol. 128, no. 4, pp. 1304–1315, 2006.